International Journal of Innovative Technology and Exploring Engineering (IJITEE)
ISSN: 2278-3075 (Online), Volume-9 Issue-3, January 2020

Data Adaptable Sparse Reconstruction for Hyperspectral Image Recovery from Compressed Measurements

Gunasheela K S, H S Prasantha

Abstract: ***Hyperspectral image compression using compressive sensing technique is very much important in the area of satellite image compression because it can greatly en hance the compression rate. The research work proposes a novel data adaptable sparse reconstruction algorithm for the reconstruction of hyperspectral images from compressive sensing measurements. In the proposed algorithm, compressive sensing technique is used for the compression of HSIs, where Gaussian i.i.d. matrix is used to generate compressive sensing measurements. The algorithm solves the optimization problem containing total variation regularization and data adaptable parameter terms. The regularization terms are added to provide hyperspectral data characteristics as priors into the objective function. The addition of priors helps in convergence of the algorithm into the desired solution. The algorithm alternatively reconstructs the end member matrix and abundance matrix instead of reconstructing the entire HSI at once, thereby reducing the computational complexity at the reconstruction process. To nullify the effect of modelling errors, debiasing is performed.***

Keywords: Hyperspectral image (HSI), Total variation, Data adaptable sparse reconstruction (DASR), Sparsity

I. INTRODUCTION

Hyperspectral image cube is a collection of images of a particular scene captured across various wavelength regions in the electromagnetic spectrum. The main applications of Hyperspectral image processing is in remote sensing applications [1][2][3][4] such as object detection, pollution monitoring, target detection in military applicationsetc. Apart from many useful applications, HSI processing is quite challenging because HSIs are huge. For example Cuprite data from AVIRIS (Airborne Visible Infrared Imaging Spectrometer) sensor of NASA has 224 bands in a hyperspectral image scene. Memory and power are the most critical resources in any airborne or satellite imaging systems. It is very difficult to store and transmit such huge amounts of data generated by Hyperspectral imaging systems. Hence compression of Hyperspectral images is very much necessary. Apart from using conventional image compression algorithms [5] for image compression, it is sensible to use compressive sensing [6] techniques to perform compression.

Revised Manuscript Received on January 30, 2020.
***** Correspondence Author
Gunasheela K S*, M.Tech. Degree Signal processing,Visveswaraya technological University, India.
H S Prasantha, Professor, Department of Electronics and Communication Engineering, Nitte Meenakshi Institute of Technology (Affiliated to VTU Belgaum), Bangalore, India.

The reason being, CS greatly increases the compression performance and also reduces the computational process at the encoder side.The Hyperspectral image compression and reconstruction methods based on compressive sensing makes use of either spatial and spectral information separately [7] or combination of spectral and spatial information. Gaussian i.i.d. matrix can be used as measurement matrix to obtain spectral compressivesampling [14]. Spectral correlation [8] or different prior information can be used to reconstruct the HSIs. Various methodologies like principal component analysis, Multi-hypothesis estimation [9] has been proposed for the reconstruction of HSIs. In general most of the techniques for HSIreconstruction perform direct reconstruction of HSI, which may cause high complexity at the computational process. To tackle this issue of high complexity in reconstructing the entire HSI, the concept of hyperspectral unmixing is introduced. According to the concept of linear mixing model for hyperspectral image, image matrix of hyperspectral image can be represented as a product of endmember matrix and abundance matrix.Based on this strategy, many algorithms have been proposed. Detailed literature survey on linear and non-linear mixing of HSIs is presented in [10]. The concept of spectral unmixing is mainly useful for multiple variations detection [11], resolutions enhancement [12] and sub pixel mapping process [13]. The hyperspectral coded aperture procedure [14] makes use of spatial pre-processing methods along with compression sensing to achieve higher compression gains with minimal error. The values of end members are very minimal compared to the raw HSI data. Hence the reconstruction of end member matrix and abundance matrix greatly enhances the speed of the computational process. It has been demonstrated that, procedures of end member and abundance matrix estimation deliver better technical solutions for compressive sensing reconstruction of HSIs [15]. The prediction of spectral characteristics by the stochastic mixing approach is presented in [16]. In [17], it is shown that, the mixed pixel spectrum of a multispectral or hyperspectral image can be disintegrated into weighted abundance linear combination of the end-members. Considering both multispectral and hyper-spectral data acquired for the same scene, the end-members are identical in nature. That is why the desirable HSI is re-build through the adaptive spectral dictionary, which extracted via the HSI data and multispectral data is used to extract the abundances. In [18], a joint non-negative matrix factorization approach that depends upon the unsupervised un-mixing, where the multispectral and hyper-spectral data are un-mixed alternatively through the non-negative matrix factorization is proposed.

Similar method has been proposed in [19], where they studied the spectral dictionary function for HSI in order to resolve higher level sparse coefficient by orthogonal identical pursuit. Whereas, in [20] authors use adaptive spectral dictionary function that corresponds to decomposition of k-singular value.In this paper, a novel DASR (Data adaptable sparse reconstruction) algorithm is proposed to perform compression and reconstruction of HSIs. Compression is performed using random Gaussian i.i.d. entries matrix as measurement matrix. Since, Compressive sensing makes use of a certain percentage of combination of input samples and not all the input samples, compression performance is greatly enhanced. To perform the reconstruction of HSI from compressive sensing measurements, the concept of hyperspectral unmixing is used. End member matrix and abundance maps are reconstructed alternatively instead of recovering the entire HSI at once which increases the computational complexity of the algorithm. Total variation regularization increases the pixel mixture and therefore not sufficient for the estimation of end members. Therefore, the data adaptable parameter is included to maximise the sparsity of abundance maps. The intensity values in Hyperspectral image have physical meaning. Reducing the bias in the abundance map is important. Therefore, debiasing technique for the restoration of TV image is incorporated. Debiasing minimizes the emerging bias at the image restoration process. End member and abundance matrix are estimated alternatively by Bregman iterative procedure.The remaining paper is organized as follows: Section II describes the proposed DASR approach for the compression and reconstruction of hyperspectral images. Section III describes the datasets, experimental setup and comparison of results in terms of quantitative metrics.

Section IV is conclusion, which briefly highlights the contributions of the paper and notes on future work and implementations. Section V contains the references.

II. PROPOSED DATA ADAPTABLE SPARSE RECONSTRUCTION (DASR) APPROACH

This section presents the proposed DASR algorithm for the compression and reconstruction of HSIs. Fig.1. represents the block diagram of the proposed algorithm. The first step is converting the Hyperspectral image cube into a 2-D matrix where each row represents a band in the hyperspectral image. Each column in the matrix corresponds to pixel vectors. Here, b is considered to be the pixel vectors such as, b=1……B. B represents the number of pixels in the hyperspectral image band. According to the concept of Linear mixing model for HSIs, HSI matrix can be represented as a product of endmember matrix and abundance matrix. Therefore the model for Hyperspectral image can be given as follows:

$$f_b = g_b + De_b \qquad (1)$$

Where, f_b denotes the spectral vector $A \times 1$ at pixel b, D denotes the indefinite mixing matrix where individual column in D defines one indefinite end-members. The vector e_b corresponds to $c \times 1$ indefinite abundance vector. The vector $g_b$stands for the noise signal. The spectral band number is represented by A. The number of end members is given by c. Therefore, the matrix notation of Eq. (1) is given as follows:

$$F = G + ED^R \qquad (2)$$

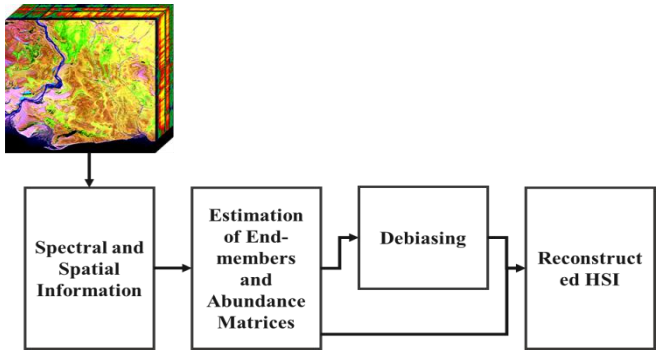

Fig.1. Proposed model block diagram

Where, F matrix stands for$F = [f_1, \ldots, f_B]^R$, R represent the row side vector. Individual row in F represent one spectral vector of a particular pixel. E represents the vector form of abundance map. The Frobenius function at E can be given as;

$$\|E\|_{FFn}^2 = \sum_{b,g} e_{b,g}^2 \qquad (3)$$

The estimated matrices E and D from equation (2) can be given as;

$$\overline{D}, \overline{E} = \arg \min_{D \geq 0, E \geq 0} K(D, E) \qquad (4)$$

Where,$g = 1, \ldots, c$ at$\|d_g\|_2^2 = 1$ and so on the cost function can be written as;

$$K(D,E) = 0.5 \sum_{b=1}^{B} \|f_b - De_b\|_2^2 + q_m \sum_{g=1}^{c} \|e_g\|_m + \beta \sum_{g=1}^{c} TV(e_g) \qquad (5)$$

The first regularizer term is given as;

$$\|e_g\|_m = \begin{cases} \sum_b |e_{(b,g)}|_0 & \text{if } m = 0 \\ \sum_b |e_{(b,g)}|^m & \text{if } 0 < m \leq 1 \end{cases} \qquad (6)$$

In addition, the data adaptable parameter $q_m$is given as;

$$q_m = \begin{cases} \frac{q^2}{2} & \text{if } m = 0 \\ q^{2-m} & \text{if } 0 < m \leq 1 \end{cases} \qquad (7)$$

The vertical dissimilarity in vectorized form is given by;

$$v_{fn}\left(H_{G_y} E_g\right) = \omega_y e_g \quad (8)$$

Where,H_{G_y}represents the first order dissimilarity matrix,$E_g = G_x \times G_y$is the abundance matrix, and$\omega_y$provide the vertical dissimilarity. The above equation can be written in vectorized form;

$$\omega_y = N_{G_x} \otimes C_{G_y} \qquad (9)$$

Here, N represents the identity matrix. The TV regularizer parameter is given by;

$$\mathrm{TV}(e_g) = \left\| \left((\omega_x e_g)^2 + (\omega_y e_g)^2 \right)^{1/2} \right\|_1 \qquad (10)$$

The TV regularization is performed as element wise process. The proposed algorithm computes one column in E, followed by onecolumn in D and vice-versa.

$$ED^R = \sum_{g=1}^{c} e_g d_g^R \qquad (11)$$

Therefore, the objective function can be redefined as

$$K_g(d,e) = 0.5\left\|H_g - ed^R\right\|_{FFn}^2 + q_m\|e\|_m + \beta \times TV(e) \qquad (12)$$

Where, the function$H_g$is given by;

$$H_g = F - E_{-g}D_{-g}^R \qquad (13)$$

Whenever the individual variable is stable except d end-members, from (4) it can be rewritten as;

$$d_g^{(p+1)} = \arg\min_{d \geq 0} K_g(d, e^p) \qquad (14)$$

Here, p denotes number of iterations, the $g = 1, \ldots, c$ at$\|d\|_2^2 = 1$ and whenever the individual variable is not fixed except d end-members then;

$$e_g^{(p+1)} = \arg\min_{e \geq 0} K_g\left(d_g^{p+1}, e\right) \qquad (15)$$

Where, $g = 1 \ldots . . c$. The end-member D estimation step is given by,

$$d_g^{(p+1)} = \arg\max_{d \geq 0} \left\|H_g - d^R e_g^p\right\|_{FFn}^2 \qquad (16)$$

Where, $g = 1, \ldots, c$ at$\|d\|_2^2 - 1 = 0$, the Bregman Iterations method [21] is used to provide optimal scaling.

$$d_g^{(p+1)} = \max\left(0, H_g^R e_g^p / \left\|H_g^R e_g^p\right\|_2\right) \qquad (17)$$

The abundance computation E is given by:

$$e_g^{(p+1)} = \arg\min_{e} 0.5\left\|H_g - ed_g^{(p+1)^R}\right\|_{FFn}^2 + q_m\|e\|_m + \beta \times TV(e) \qquad (18)$$

So, the problem of convex minimization can be rewritten as;

$$\min_{l \geq 0} 0.5\, S\|l - t\|_2^2 + \left\|\sqrt{W_x^2 + W_y^2}\right\|_1 + q_m'\|l\|_m, \qquad (19)$$

Where,$W_x$is equivalent to$\omega_x l$ and$W_y$is equivalent to$\omega_y l$,$q_m' = q_m/\beta$, $S = \frac{1}{\beta}$and $l = e_g$. The complete minimization problem is solved using Bregman Iterations method [21]. The t parameter is computed as;

$$t = H_g d_g^{(p+1)} \qquad (20)$$

The TV computation process is used to tackle the problem of bias, where the outcome is scaled to get similar variance in the non-regularized solution. The non-regularized solution is denoted as α. So the de-biasing function δ can be written as;

$$\delta(e) = \max\left(0, (e - \bar{e}) \times \left(\varphi_\alpha/\varphi_e\right) + \bar{e}\right) \qquad (21)$$

Where,$\bar{e}$stands for the mean value of e,$\varphi_\alpha$and$\varphi_e$represents the standard deviations value of α and e, which will be great if$\varphi_G \ll \varphi_e$and$\varphi_G$stands for the noise variance.Table 1 shows the algorithm 1 that is used to get optimal reconstruction of HSIs with minimal amount of error, this process alters between one column in D and one column in E for the estimation using (17). If the de-biasing is need to perform then it will start from S-5 in algorithm-1. Also the algorithm get suspended whenever it meet with the maximal allowed iteration or through computation of the relative differences between E and D.

Table.1. Algorithm 1

S-1:	Initialize F, c, m, q and β, also value D and E to zero
S-2:	In starting step $p = 0$
S-3:	Start: till some stopping conditions not met
S-4:	for $g = 1, \ldots, c$ do
S-5:	Compute (15)
S-6:	$d_g^{(p+1)} = \arg\min_{d \geq 0} K_g(d, e^{p+1})$
S-7:	End for loop
S-8:	Increasing the P value after each interval
S-9:	Stop

III. EXPERIMENTAL RESULTS AND ANALYSIS

In order to evaluate the performance of the proposed method, two hyperspectral image datasets has been considered. The Pavia dataset [22],and three Cuprite [23] scenes of AVIRIS sensor is considered for experimentation. All these Hyperspectral images are made up of different kinds of end member signature which helps in proper evaluation of the proposed algorithm.The Pavia dataset is collected by the ROSIS (Reflective optics system imaging spectrometer) sensor. ROSIS sensor captures the scene across 115 bands in the electromagnetic spectrum. The spatial size of each band is 610 by 340. The spatial resolution in each band is 1.3m at each pixel. The three scenes of Cuprite corresponds to the first three images of the online cuprite reflectance data. These scenes are captured by the Airborne AVIRIS (Airborne Visible Infrared Imaging Spectrometer) sensor. AVIRIS sensor captures the Hyperspectral image across 224 different narrow wavelength regions in 0.4 to 2.5μm range in the electromagnetic spectrum. The spectral width is around 10nm. Thus the cuprite dataset consists of 224 spectral bands. The spatial resolution in each band is 20m at each pixel. The proposed algorithms are simulated in MATLAB 2016b to demonstrate the reconstruction accuracy. Here the system configuration is 8GB RAM, 1TB ROM, Intel i9 processor, 2GB NVidia Graphics card with the latest operating system windows 10.Three quantitative metrics has been used to validate the performance of the proposed algorithms. They are PSNR (Peak signal to noise ratio)[24], SSIM (Structural similarity index measure) [25] and spectral angle mapper (SAM) [26]. In order to evaluate the reconstruction performance of the proposed DASR algorithm, four reconstruction models are considered for the comparison purpose. The minimization TV (min-TV) approach is initially considered with magic package and quadratic constraints [27], where it takes the random Gaussian matrix as the spatial measurement matrix. It makes use of image gradient sparseness in the process of reconstruction, and conduct the reconstruction through optimization of TV minimization. Also the 3-dimensional CS (3DCS) model [28] is considered, where the images are sampled using 3-dimensional convolution process and images are reconstructed through 3-dimensional TV minimization of hyper-spectral data samples. The compressive projection PCA (CPPCA) has been proposed in [29], it make use of random Gaussian matrix in order to sample individual pixel vector. At the process of reconstruction, PCA is introduced instead of sparse constraints for the optimized reconstruction problem. In addition, the Spatial-Spectral Compressed Reconstruction based Spectral-Unmixing (SSCR_SU) is proposed in [30], the SSCR_SU algorithm make use of random Gaussian matrix and spatial coherent matrix to get the information of spatial and spectral data. The joint optimization problems for abundance estimation and end-member extraction are used to reconstructed images.

Table 2 shows the PSNR values obtained using the DASR algorithm for Cuprite scene 1 data. The results obtained are compared with four different algorithms such as min-TV, 3 DCS, CPPCA and SSCR_SU. First column represents the Sampling rate. At 0.1 sampling rate PSNR obtained using the DASR algorithm is 59.4087 which is 33.5%, 74%, 80% better compared to SSCR_SU, 3DCS and min-TV algorithms respectively.Table 3 shows the PSNR values obtained for Cuprite scene 2 data. The proposed algorithm performs 30.75%, 28.94%, and 40.56% better than the SSCR_SU at 0.1,0.2 and 0.5 sampling rate respectively. Table 4 shows the PSNR values obtained for Cuprite scene 3 data. The proposed algorithm performs 37.2%, 36.02%, 48.31% better than SSCR_SU algorithm at 0.1, 0.2, and 0.5 sampling rate respectively. Table 5 shows the PSNR values obtained for Pavia data. The proposed algorithm performs 9.32%, 6.91%, and 12.38% better than the SSCR_SU algorithm at 0.1,0.2 and 0.5 sampling rate respectively. Table 6 shows the SSIM values obtained using DASR algorithm for Cuprite scene 1 data. The results obtained are compared with four different algorithms such as min-TV, 3 DCS, CPPCA and SSCR_SU. First column represents the Sampling rate. At 0.1 sampling rate, SSIM value using DASR algorithm is 0.9991 which is 0.5 % greater than the better performing algorithms among four algorithms chosen for comparison. At 0.5 sampling rate, proposed algorithm performs 0.5 % better than the SSCR_SU algorithm.Table 7 shows the SSIM values obtained for Cuprite scene 2 data. The proposed algorithm performs 0.61 % and 0.31 % better than SSCR_SU at 0.1 sampling rate and 0.5 sampling rate respectively. Table 8 shows the SSIM values obtained for Cuprite scene 3 data. The proposed algorithm performs 0.6 %, 0.4 %, 0.37 % better than SSCR_SU algorithm at 0.1, 0.2 and 0.5 sampling rates respectively.Similarly Table 9 shows the SSIM values obtained for PaviaU data. The proposed algorithm performs 2%, 1.3%, and 0.3% better than the SSCR_SU algorithm at 0.1,0.2, and 0.5 sampling rates respectively.Fig. 2 shows the SAM values obtained using DASR algorithm for Cuprite scene 1, Cuprite scene 2, Cuprite scene 3 and Pavia data. The average SAM value obtained for cuprite scenes is 0.2131 at 0.1 sampling rate. The average value of SAM for cuprite scenes at 0.5 sampling rate is 0.0434. The decrease in SAM value indicates the increase in spectral similarity with increase in sampling rate. The SAM value for Pavia data at 0.1 sampling rate is 1.82. The SAM value for Pavia data at 0.5 sampling rate is 0.51. Fig.3 shows Reconstructed HSIs for Cuprite_S2 at 0.2 sampling rate by four algorithms; the first row consists of 50th band images, where (a),(b),(c),(d) represent 3DCS , CPPCA , SSCR_SU and DASR algorithms respectively. The second row consists of 80th band images, where (e),(f),(g),(h)represent 3DCS, CPPCA, SSCR_SU and DASR algorithms respectively. Similarly, Fig. 4 shows reconstructed HSIs for Pavia University at 0.2 sampling rate by four algorithms; where the first row represents 50th band images and the second row represents 80th band images.

Table2: PSNR value for Cuprite S1

Sampling Rate	Min-TV	3DCS	CPPCA	SSCR_SU	DASR
0.1	33	34	12.5	44.5	59.4087
0.2	34	36.8	42	46.7	62.0041
0.3	35.4	38	43	47.1	64.2268
0.4	36.7	40.1	44	47.5	66.501
0.5	37	41.2	45	48	70.32

Table 3: PSNR value for Cuprite S2

Sampling Rate	Min-TV	3DCS	CPPCA	SSCR_SU	DASR
0.1	28	34.2	14	44.5	58.1869
0.2	30	37	41	47.6	61.3788
0.3	31	40	43	48	63.95
0.4	32	42.5	45	49	66.2836
0.5	34	44	46	50	70.28

TableError! No text of specified style in document.**: PSNR value for Cuprite S3**

Sampling Rate	Min-TV	3DCS	CPPCA	SSCR_SU	DASR
0.1	25.1	33	12.2	43	58.997
0.2	25	36	38	45.3	61.62
0.3	26.2	37.6	42	46	64.04
0.4	27.4	39	44	46.9	66.31
0.5	28.3	40.5	44.8	47.4	70.3

Table 5: PSNR value for PaviaU

Sampling Rate	Min-TV	3DCS	CPPCA	SSCR_SU	DASR
0.1	21	34	19.8	40.2	43.95
0.2	22	37	35.2	45	48.11
0.3	23.4	42	37	47.4	50.06
0.4	25.1	43	41.7	48	52.93
0.5	26	45	43.5	49	55.07

Table 6:SSIM score for Cuprite S1

Sampling Rate	Min-TV	3DCS	CPPCA	SSCR_SU	DASR
0.1	0.7927	0.9566	0.1449	0.9932	0.9991
0.2	0.8427	0.9732	0.9908	0.9947	0.9995
0.3	0.8705	0.9835	0.994	0.9953	0.9997
0.4	0.8981	0.9879	0.995	0.9957	0.9998
0.5	0.9223	0.9915	0.9957	0.9959	0.9999

Table 7: SSIM score for Cuprite S2

Sampling Rate	Min-TV	3DCS	CPPCA	SSCR_SU	DASR
0.1	0.6302	0.9302	0.1746	0.9929	0.9991
0.2	0.7021	0.9634	0.9891	0.9955	0.9995
0.3	0.754	0.9797	0.9937	0.9961	0.9997
0.4	0.8027	0.9864	0.9956	0.9965	0.9998
0.5	0.8482	0.9911	0.9963	0.9967	0.9999

Table 8: SSIM score for Cuprite S3

Sampling Rate	Min-TV	3DCS	CPPCA	SSCR_SU	DASR
0.1	0.7319	0.9484	0.1529	0.993	0.9991
0.2	0.7886	0.9693	0.9874	0.995	0.9995
0.3	0.8242	0.9815	0.9925	0.9955	0.9997
0.4	0.8628	0.9868	0.995	0.996	0.9998
0.5	0.8958	0.991	0.9957	0.9962	0.9999

Table 9: SSIM score at PaviaU Dataset

Sampling Rate	Min-TV	3DCS	CPPCA	SSCR_SU	DASR
0.1	0.3552	0.906	0.423	0.9761	0.9971
0.2	0.4411	0.9565	0.944	0.9876	0.9988
0.3	0.5244	0.9759	0.9725	0.9931	0.9993
0.4	0.6149	0.9838	0.9845	0.9948	0.9996
0.5	0.7055	0.989	0.9915	0.996	0.9998

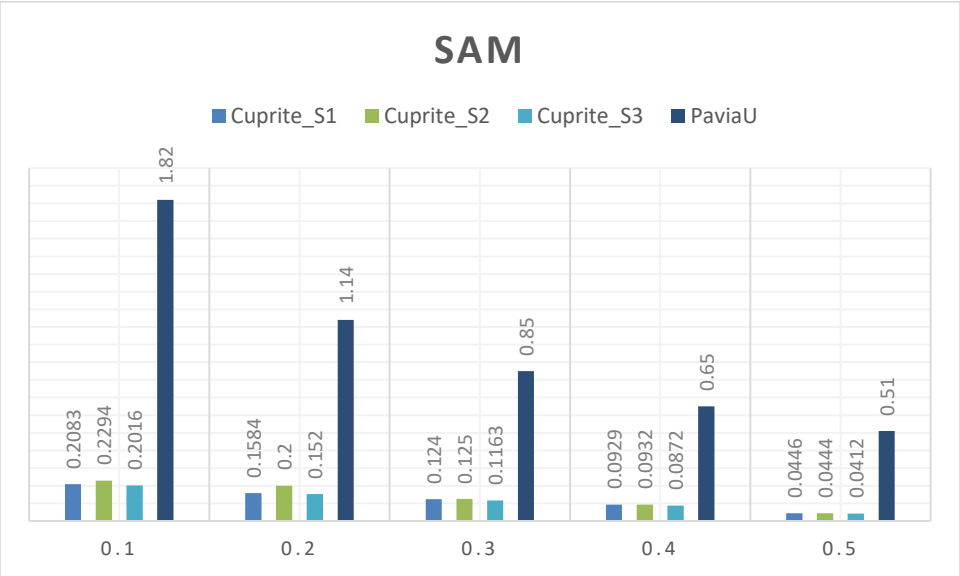

Fig. 2:SAM value for different HSI dataset

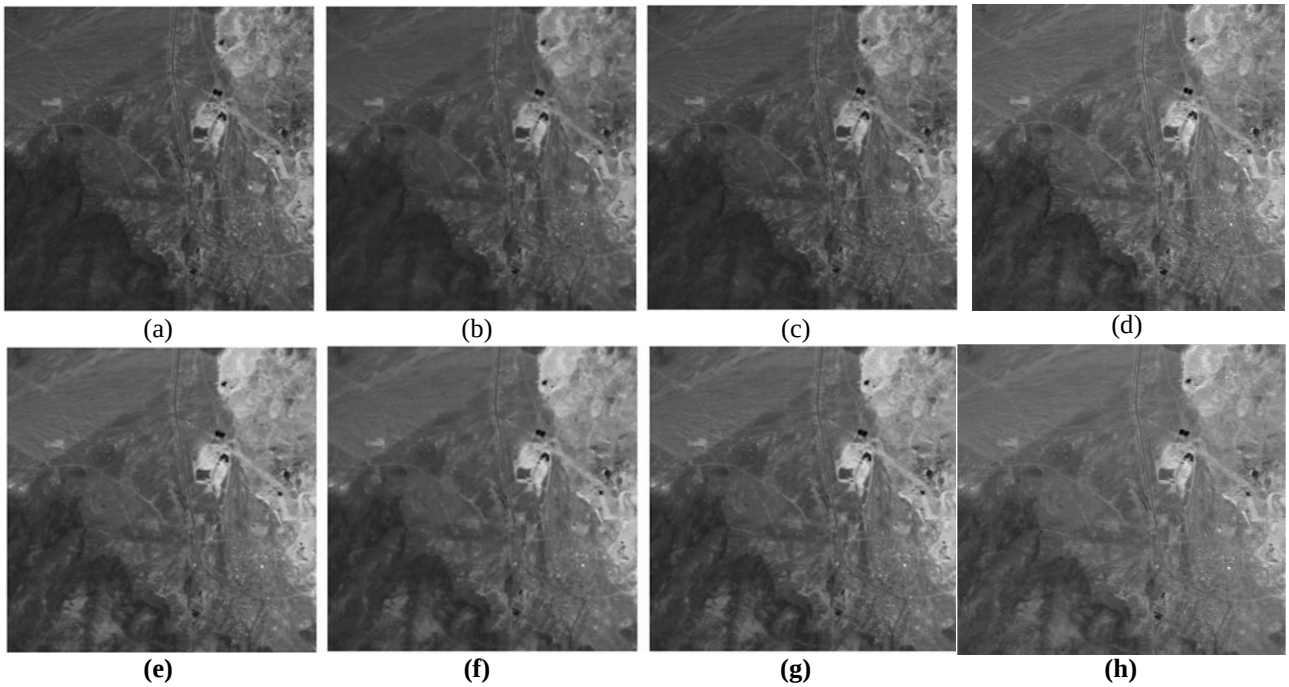

Fig. 3: Reconstructed HSIs for Cuprite_S2 at 0.2 sampling rate by four algorithms; the first row for 50th band images and the second row for 80th band images

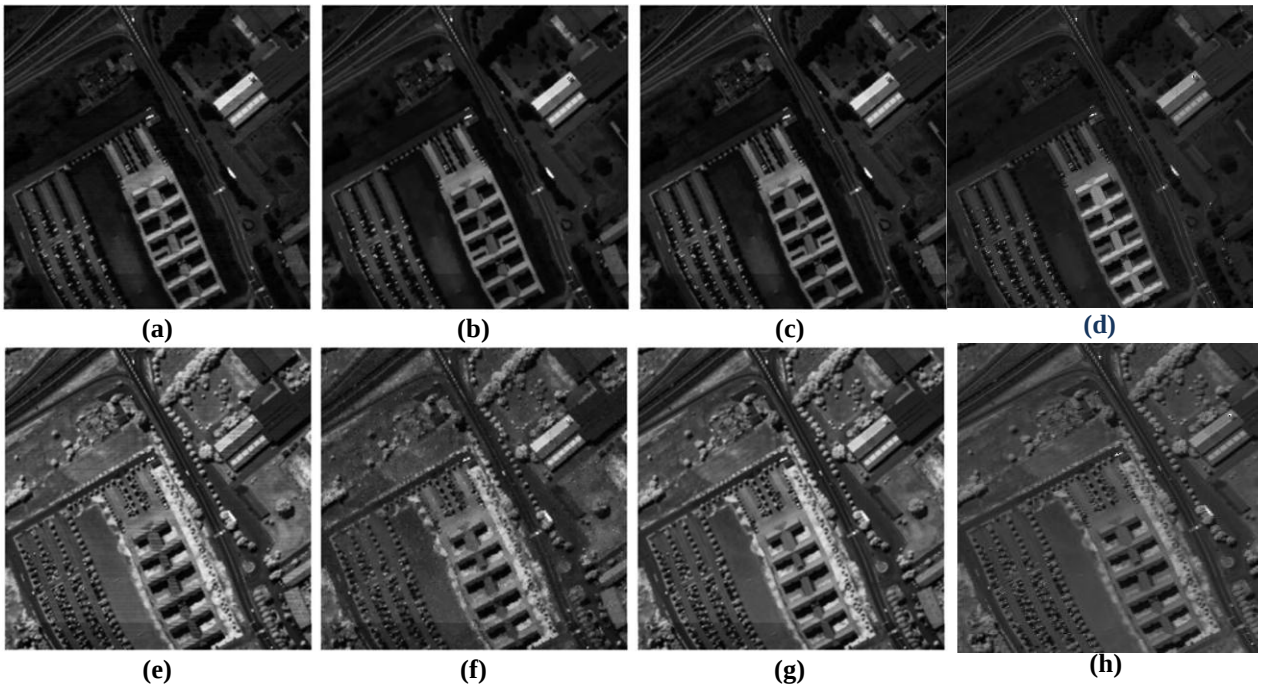

Fig. 4: Reconstructed HSIs for Pavia dataset at 0.2 sampling rate by four algorithms; the first row represents 50th band images and the second **row represents 80th band images:**

IV. CONCLUSION

In this paper, the novel data adaptable sparse reconstruction (DASR) algorithm for HSI reconstruction from compressed measurements is proposed. The objective function of the optimization problem contains two priors, one is total variation regularization term and the other one is data adaptable term. The TV regularizer and data adaptable parameter is combined here under an un-mixing process to complement each other and provide important hyperspectral image data characteristics. The TV regularizer increasesthe pixels mixture, so alone it is not sufficient to estimate end-members. Therefore, data adaptable parameter is added into the objective functionto provide smooth abundance by retaining discontinuities. The data adaptable parameter minimizes the pixels mixture by maximizing the sparsity of abundance maps. The end member matrix and abundance maps are alternatively reconstructed thereby reducing the computational complexity of otherwise reconstructing the whole hyperspectral image at once. The optimization problem is solved using Bregman method. Analysing the result, it is evident that the proposed DASR algorithm has performed well at each sampling rate and achieved better SSIM score and PSNR values.

This shows the accuracy and efficiency of the proposed model with respect to different HSI datasets. In future to further accelerate the reconstruction process, the algorithm can be implemented using GPUS.

REFERENCES

1. M. S. Stefanou and J. P. Kerekes,Apr. 2010, "Image-derived prediction of spectralimage utility for target detection applications," *IEEE Trans. Geosci. Remote Sens.*, vol. 48, no. 4, pp. 1827–1833.
2. N K Patel, C. Patnaik, S. Dutta, 2001, A. M. Shekh, and A. J. Dave, "Studyof crop growth parameters using airborne imaging spectrometer data," *Int. J. Remote Sens.*, vol. 22, no. 12, pp. 2401–2411.
3. M.T. Eismann, A. D. Stocker, and N. M. Nasrabadi, Jun. 2009,"Automatedhyperspectral cueing for civilian search and rescue," *Proc. IEEE*, vol. 97, no. 6, pp. 1031–1055.
4. M. Borengasser, W.S. Hungate, and R. Watkins, Hyperspectral Remote sensing Principles and Applications. Boca Raton FL,USA CRC Press
5. Gunasheela K S, H S Prasantha, "Satellite image compression-detailed survey of the algorithms", Proceedings of ICCR in LNNS Springer, 2017, vol. 14, pp. 187-198.
6. Gunasheela K S, H S Prasantha, "Compressive sensing for image compression: survey of algorithms", Proceedings of Emerging Research in Computing, Information, Communication and Applications, ERCICA, Springer publication, Bengaluru, 2018
7. L. Wang and Y. Feng, 2016 ,"Compressed sampling reconstruction of hyperspectral images based on spectral prediction," IEEJ. Trans. Electr, vol. 11, no. 1, pp. 63–72.
8. Y. Jia, Y. Feng, and Z. Wang,2015, "Reconstructing hyperspectral images fromcompressivesensorsviaexploitingmultiplepriors,"Spectrosc.Lett., vol. 48, no. 1, pp. 22–26.
9. C. Chen, W. Li, E. W. Tramel, and J. E. Fowler, Jan. 2014 ,"Reconstruction of hyperspectral imagery from random projections using multi-hypothesis prediction," IEEE Trans. Geosci. Remote Sens., vol 52, no. 1, pp. 365– 374.
10. J. M. Bioucas-Dias, A. Plaza, N. Dobigeon, M. Parente, Q. Du, and P.Gader, "Hyper-spectral un-mixing overview: Geometrical, statistical, and sparse regression-based approaches," IEEE J. Sel. Top. Appl. Earth Obs. Remote Sens., vol. 5, no. 2, pp. 354–379, Apr. 2012.
11. S. Liu, L. Bruzzone, F. Bovolo, and P. Du, "Unsupervised multitemporal spectral unmixing for detecting multiple changes in hyper-spectral images," IEEE Trans. Geosci. Remote Sens., vol. 54, no. 5, pp. 2733–2748, May 2016.
12. B. Mohamed, M. He, and S. Mei, "Hyperspectral image resolution enhancement using high-resolution multispectral image based on spectral unmixing," IEEE J. Sel. Top. Appl. Earth Obs. Remote Sens., vol. 52, no. 10, pp. 6574–6583, Oct. 2014.
13. X. Xu, X. Tong, A. Plaza, Y. Zhong, H. Xie, and L. Zhang, "Using linear spectral unmixing for subpixel mapping of hyperspectral imagery: A quantitative assessment," IEEE J. Sel. Top. Appl. Earth Obs. Remote Sens., vol. 10, no. 4, pp. 1589–1600, Apr. 2017.
14. G.Martin, J.M.Bioucas-Dias, and A.Plaza, "HYCA:Anewtechniquefor hyperspectral compressive sensing," IEEE Trans. Geosci. Remote Sens., vol. 53, no. 5, pp. 2819–2831, May 2015.
15. Gunasheela K S, H S Prasantha, "A Novel DASR Approach for reconstruction of Hyper-spectral images ", in press, ICTCS, Springer publication, Udaipur, December 2019.
16. M. T. Eismann and R. C. Hardie, "Hyper-spectral resolution enhancement using high-resolution multispectral imagery with arbitrary response functions," IEEE Trans. Geosci. Remote Sens., vol. 43, no. 3, pp. 455–465, Mar. 2005.
17. J. M. Bioucas-Dias et al., "Hyper-spectral un-mixing overview: Geometrical, statistical, and sparse regression-based approaches," IEEE J. Sel. Topics Appl. Earth Observ. Remote Sens., vol. 5, no. 2, pp. 354–379, Apr. 2012.
18. N. Yokoya, T. Yairi, and A. Iwasaki, "Coupled nonnegative matrix factorization un-mixing for hyper-spectral and multispectral data fusion," IEEE Trans. Geosci. Remote Sens., vol. 50, no. 2, pp. 528–537, Feb. 2012.
19. R. Kawakami, Y. Matsushita, J. Wright, M. Ben-Ezra, Y.-W. Tai, and K. Ikeuchi, "High-resolution hyper-spectral imaging via matrix factorization," in Proc. IEEE Comput. Vis. Pattern Recognit. (CVPR), Jun. 2011, pp. 2329–2336.
20. B. Huang, H. Song, H. Cui, J. Peng, and Z. Xu, "Spatial and spectral image fusion using sparse matrix factorization," IEEE Trans. Geosci. Remote Sens., vol. 52, no. 3, pp. 1693–1704, Mar. 2014.
21. K. S. Gunasheela and H. S. Prasantha, "Sparse Reconstruction of Hyperspectral Image using Bregman Iterations," 2018 Second International Conference on Advances in Electronics, Computers and Communications (ICAECC), Bangalore, 2018, pp. 1-7.
22. Grupo de Inteligencia Computacional, Hyperspectral Remote Sensing Scenes. 2014. [Online]. Available: http://www.ehu.eus/ccwintco/index.php title = Hyperspectral Remote Sensing Scenes
23. G. Vane et al., AVIRIS free data. 1997. [Online]. Available: http://aviris.jpl.nasa.gov/data/free_data.html
24. Y. Peng, D. Meng, Z. Xu, C. Gao, Y. Yang, and B. Zhang, 2014 ,"Decomposable nonlocal tensor dictionary learning for multispectral image denoising," in Proc. IEEE CVPR, , pp. 2949–2956.
25. Z.Wang, A. C. Bovik, H. R. Sheikh, and E. P. Simoncelli,Apr. 2004, "Image quality assessment: From error visibility to structural similarity," IEEE Trans. Image Process., vol. 13, no. 4, pp. 600–612,.
26. R. H. Yuhas, 1990 ,"Determination of semi-arid landscape endmembers and seasonal trends using convex geometry spectral unmixing techniques," Ratio, vol. 4, p. 22,
27. E. Cand`es and J. Romberg, l1-magic: Recovery of sparse signals via convex programming. 2005. [Online]. Available: https://statweb.stanford.edu/~candes/l1magic/downloads/l1magic.pdf
28. L.Wang and Y. Feng, "Hyperspectral imaging via three-dimensional compressed sampling," Paper presented at the Int. Conf. Adv. Comput. Sci.Electron. Inf., Beijing, China, pp. 25–26, Jul. 2013.
29. J. E. Fowler, "Compressive projection principal component analysis," IEEE Trans. Image Process., vol. 18, no. 10, pp. 2230–2242, Oct. 2009.
30. L. Wang, Y. Feng, Y. Gao, Z. Wang and M. He, "Compressed Sensing Reconstruction of Hyperspectral Images Based on Spectral Unmixing," in IEEE Journal of Selected Topics in Applied Earth Observations and Remote Sensing, vol. 11, no. 4, pp. 1266-1284, April 2018.

AURHOR PROFILE

Gunasheela K S received the B.E. degree in Electronics and Communication Engineering and the M.Tech. Degree in Signal processing from Visveswaraya technological University, India in the year 2012 and 2014 respectively. She is currently working towards the Ph.D. degree in the area of hyperspectral image compression at Nitte Meenakshi institute of technology affiliated to VTU, India. Her research interests include compressed sensing, hyperspectral image processing, optimization and computer vision.

Dr. Prasantha H S received Bachelor degree from Bangalore University, Master Degree from V.T.U, Belgaum, and PhD from Anna University, Chennai, in the area of Signal and Image Processing. He has 20+ years of teaching and research experience. His research interest includes Multimedia and Signal Processing. He has published more than 35 papers in International conferences and Journals. He is a reviewer for various reputed conferences and Journals. He is currently guiding four students for their research program under VTU. Currently, he is working as a Professor in the department of Electronics and Communication Engineering, Nitte Meenakshi Institute of Technology (Affiliated to VTU Belgaum), Bangalore.